In-beam and α-decay spectroscopy of ^{191}Po and evidence for triple shape coexistence at low energy in the daughter nucleus ^{187}Pb

A. N. Andreyev,* M. Huyse, K. Van de Vel, and P. Van Duppen
Instituut voor Kern- en Stralingsfysica, K.U. Leuven, Celestijnenlaan 200 D, B-3001 Leuven, Belgium

O. Dorvaux, P. Greenlees, K. Helariutta, P. Jones, R. Julin, S. Juutinen, H. Kettunen, P. Kuusiniemi, M. Leino, M. Muikku, P. Nieminen, P. Rahkila, and J. Uusitalo
Department of Physics, University of Jyväskylä, FIN-40351 Jyväskylä, Finland

R. Wyss
Department of Physics, Royal Institute of Technology, 106 91 Stockholm, Sweden

K. Hauschild and Y. Le Coz
DAPNIA/SPhN, CEA Saclay, F91191 Gif Sur Yvette Cedex, France

(Received 12 March 2001; revised manuscript received 11 April 2002; published 26 July 2002)

Prompt γ rays have been observed for the first time from the neutron-deficient nucleus ^{191}Po using the recoil-decay tagging technique at the RITU gas-filled separator. In addition improved α decay data have been measured for ^{191}Po and its daughter product ^{187}Pb. The complementary γ- and α-decay data point to the onset of oblate deformation in the light odd-mass Po nuclei by approaching the neutron midshell at $N=104$. The pattern of the favored and unfavored states observed on top of the $13/2^+$ isomer in ^{191}Po indicates a change from the weak-coupling towards the strong-coupling scheme in ^{191m}Po. In the daughter nucleus ^{187}Pb, the $13/2^+$ and $3/2^-$ isomeric states become degenerate within the experimental accuracy. Evidence for triple shape coexistence at low energy has been found in the high-spin isomer in ^{187}Pb. The results are supported by potential-energy surface calculations and by particle-plus-rotor calculations.

DOI: 10.1103/PhysRevC.66.014313 PACS number(s): 27.80.+w, 23.60.+e, 25.70.−z, 27.70.+q

I. INTRODUCTION

In the last decade the evolution of the collective motion and shape coexistence phenomena at low excitation energy in the neutron-deficient polonium isotopes has become the subject of intensive experimental and theoretical studies; see [1,2] and references therein for a recent review. The excited states in the even-mass polonium nuclei down to $N=106$ (^{190}Po [3]) have been extensively studied both by in- and off-beam γ-ray detection [2–10] and by α- and β-decay methods (see [11,12] and references therein). With only two additional protons above the spherical shell closure at $Z=82$ these nuclei demonstrate an interesting interplay between the single-particle and collective degrees of freedom, such as the textbook two-nucleon shell-model multiplets close to $N=126$, harmonic and anharmonic quadrupole or even octupole collective structures [5–7] coexisting with deformed intruder states around $N=114$ [12], and, finally, a gradual transition to more rotationlike deformed structures in the lighter isotopes with $N\leqslant 110$ [3,8–10].

Studies of the odd-mass Po nuclei can provide a crucial test of the development of collectivity close to the shell closure at $Z=82$. The coupling of an odd neutron to the even-even core can change in a dramatic way the structure and the relative positions of the different configurations. This is best illustrated by the pronounced odd-even staggering in the mean square charge radii of the platinum [13] and mercury nuclei [14] around $N=101$–107 as observed by optical and laser spectroscopy. In the odd-mass Po nuclei with N$<$126 normal parity $3p_{3/2}$ and $2f_{5/2}$ and unique parity $1i_{13/2}$ neutron orbitals are responsible for the lowest states, and below $A=201$ $3/2^-$ and $13/2^+$ isomeric states have been identified in all odd-mass Po nuclei down to ^{191}Po [4,15,16]. Furthermore, recent in-beam studies of the light odd-mass polonium isotopes have identified the lowest positive parity states, built on top of the $13/2^+$ isomer in ^{193,195,197}Po [10,17], and have shown that the level pattern of the odd-mass nuclei follows closely the downward behavior of the excitation energies in the even-even neighbors when going towards more neutron-deficient nuclei. This has been interpreted as a weak coupling of the odd $1i_{13/2}$ neutron to the low-lying states of the even-even core [10,17]. Furthermore, in [10] in addition to the favored $13/2^+$-$17/2^+$-$21/2^+$-$\cdots$ band, an indication for the unfavored $15/2^+$-$19/2^+$-$\cdots$ band, built on top of the $13/2^+$ state, has been observed in ^{193,195}Po. In these nuclei the positions of the unfavored states relative to the favored ones indicate a trend towards a strong-coupling scheme in agreement with the picture of the onset of oblate deformation at low spin in the polonium nuclei close to $N=108$ [1].

In a recent Letter we reported on an α-decay study of the nucleus ^{191}Po ($N=107$) [16]. The experiment was performed at the RITU gas-filled separator [18] and for the first time two α-decaying isomeric states were identified in ^{191}Po

*Present address: Department of Physics, Oliver Lodge Laboratory, University of Liverpool, P.O. Box 147, Liverpool, L69 7ZE, United Kingdom.

(with tentative spin and parity of $13/2^+$ and $3/2^-$) with almost equal α transition energies [7378(15) keV and 7334(15) keV], but totally different half-life values [98(8) ms and 22(1) ms]. The dramatic difference in half-life of the two isomeric states in ^{191}Po was explained in the shape coexisting approach through the action of multiparticle multihole intruder orbitals, leading to a pronounced shape staggering between the $13/2^+$ and $3/2^-$ isomeric states in ^{191}Po, a conclusion which was supported by potential energy surface calculations [16]. In addition, from observation of the fine structure in the α decay of ^{191m,g}Po, intruder states in the daughter ^{187m,g}Pb have been found.

A follow-up experiment was aimed at an in-beam study of ^{191}Po with the goal to obtain complementary data on the structure of the $13/2^+$ and $3/2^-$ isomers and to extend the systematics of the excited states to even more neutron-deficient Po nuclei. Furthermore, improved data on the α-decay properties of ^{191}Po and its daughter product ^{187}Pb could be obtained as well. The present paper reports on the complementary in-beam and α-decay data for ^{191}Po that resulted from this study. After a short description of the experimental setup (Sec. II), the results on the α decay of ^{191}Po (Sec. III A) and on the γ decay of the excited states of ^{191}Po (Sec. III B) are presented. Section IV presents a short description of the potential-energy surface (PES) calculations and the particle-plus-rotor (PPR) calculations (Sec. IV A), along with a discussion of the configuration assignments and shape staggering in ^{191m,g}Po (Sec. IV B), of the energy systematics of the structure built on the $13/2^+$ isomer (Sec. IV C), and of possible evidence for a prolate-oblate-spherical shape coexistence in the high-spin isomer in ^{187}Pb (Sec. IV D). Conclusions are given in Sec. V.

II. EXPERIMENTAL SETUP

The experiment was performed at the Accelerator Laboratory of the University of Jyväskylä (JYFL). Details of the experimental equipment and method were given in [10] and here we present only the specific features, pertinent to our experiment. The gas-filled recoil separator RITU [18], coupled to the Jurosphere Ge array around the target, was used.

^{191}Po nuclei were produced in the complete fusion reaction ^{142}Nd(^{52}Cr,3n)^{191}Po at a beam energy of $E(^{52}\mathrm{Cr}) = 236(1)$ MeV in front of the target, which corresponds to the maximum of the excitation function for this reaction measured in [19]. A continuous beam of ^{52}Cr, delivered by the $K=130$ cyclotron, was used with an average intensity of about 12 pnA, limited by the counting rates of about 10 kHz in the Ge detectors of the Jurosphere array. The enriched metallic ^{142}Nd (99.8% enrichment, 470 μg/cm^2 thickness) was evaporated onto a carbon backing of 50 μg/cm^2 thickness and covered with an additional layer of 10 μg/cm^2 of carbon.

The fusion-evaporation residues, after passing through the RITU separator, were implanted into a position-sensitive silicon strip detector (PSSD) installed in the focal plane, 4.5 m from the target position. A recently developed thin gas detector [20] installed in front of the PSSD allowed us to discriminate fusion products from scattered beam particles and to distinguish implantation of recoils from their subsequent α decays in the PSSD. As a result of its good position resolution ($\approx$0.5 mm for the recoil-α pairs), the PSSD can be considered as composed of a few hundred independent detectors or pixels. This enables the recoils to be correlated with their subsequent α decays and thus to use the recoil-decay tagging (RDT) method [21,22], in which the characteristic particle (in this case α) decay of the recoils at the focal plane is used to tag and to identify prompt γ rays emitted by these recoils at the target position. At the focal plane five Ge detectors were installed in close geometry surrounding the detector chamber perpendicularly to its walls. These detectors allowed measurements of the decays of relatively long-lived isomeric states with half-life values of the order of $\sim$0.5–10 μs, which survived during the flight time through the separator (about 0.6 μs). Moreover, this system allowed measurements of prompt and delayed (up to 10 μs) $\alpha-\gamma$- and α–x-ray coincidences. Energy calibration and absolute efficiency determination of these Ge detectors were performed by using an intensity-calibrated ^{60}Co source and mixed ^{152}Eu/^{133}Ba γ sources. Identification of the nuclides was based on the well-known α-decay energies and half-life values.

Prompt γ rays at the target position were detected by the Jurosphere Ge array which consisted of 10 TESSA type detectors and 13 Eurogam phase I type detectors with a total photo peak efficiency of about 1.5% at 1.3 MeV.

Energy, position, and detection time signals from the PSSD for the recoils and α particles, along with the γ-ray energies and detection times from the Ge detectors at the target and at the focal plane, were recorded event by event on the tape. The data were written on the tape only if any event in the PSSD was observed.

III. EXPERIMENTAL RESULTS

A. α decay of ^{191}Po

1. Fine structure α decays of ^{191m,g}Po

The decay properties of ^{191m,g}Po, deduced from the previous experiment, were discussed in detail in [16] and we will refer extensively to this paper. In the present experiment we collected about 7 times more statistics for each isomer in ^{191}Po, compared to [16], and as a result of better background conditions, we obtained improved α-decay data, which are mainly discussed in this section.

A part of the energy spectrum of the α particles, collected in this study, is shown in Fig. 1. The inset in Fig. 1 shows an expanded part of the spectrum (7100–7500 keV). This figure should be compared to Fig. 1 of Ref. [16] in which the ^{160}Dy(^{36}Ar,5n)^{191}Po reaction was used. As a result of better target enrichment in this experiment (99.8% for the ^{142}Nd target compared to 67.1% for the ^{160}Dy target in [16]), the background from the heavier Bi and Po isotopes was much lower. This, together with the lower beam intensity, compared to [16], resulted in a lower number of random correlations in the recoil-α_1(^{191}Po) and recoil-α_1(^{191}Po)-α_2(^{187}Pb) correlation analysis. Consequently, we

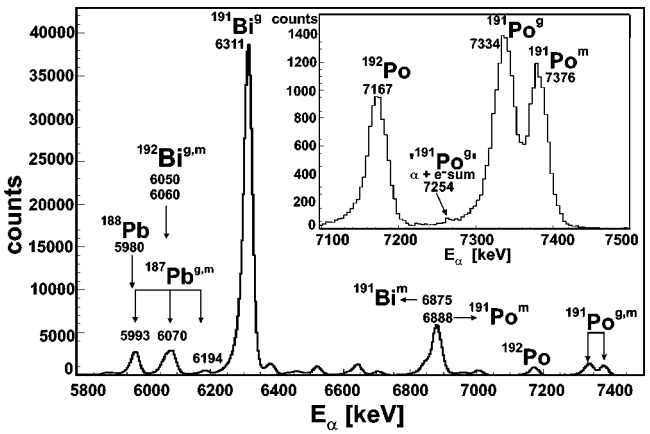

FIG. 1. Singles α-particles energy spectrum for the ^{142}Nd(^{52}Cr,3n)^{191}Po reaction collected at a beam energy of 236(1) MeV. The inset shows an expanded part of the spectrum for the 7100–7500 keV α-energy interval. Some α peaks are labeled with the α-decay energy (in keV) and the isotope the α decay belongs to.

confirmed the existence of two isomeric states in ^{191}Po and, based on higher statistics and longer correlation intervals, we deduced more precise values: $E_\alpha = 7334(5)$ keV, $T_{1/2} = 22(1)$ ms for the low-spin isomeric state in ^{191}Po and $E_\alpha = 7376(5)$ keV, $T_{1/2} = 93(3)$ ms for the high-spin isomeric state in ^{191}Po. As will be shown below, the high-spin isomer (presumably $13/2^+$) was found about 40 keV above the low-spin isomer (presumably $3/2^-$), thus establishing the latter as the ground state in ^{191}Po.

Fine structure lines in the α decay of ^{191m,g}Po were identified by analyzing the prompt [$\Delta T(\alpha\text{-}\gamma) \leqslant 100$ ns] α-γ coincidence matrix, shown in Fig. 2 (cf. the prompt α-γ matrix in Fig. 3 of Ref. [16]). Observation of the 6966(10)-375(1) keV and 6888(5)-494(1) keV α-γ coincident pairs confirms previously identified [16] fine structure α decays with $E_\alpha = 6960(15)$ keV in ^{191g}Po and $E_\alpha = 6888(15)$ keV in

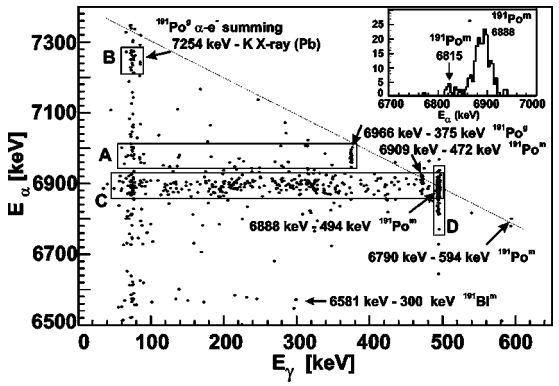

FIG. 2. Prompt $\Delta T(\alpha\text{-}\gamma) \leqslant 100$ ns α-γ coincidence matrix. Arrows point to α-γ coincidence events that are labeled with the α and the γ decay energy (in keV) and the isotope the α decay belongs to. The dashed line indicates the line of the constant $Q_{\alpha,sum} = Q_\alpha + E_\gamma = 7534$ keV value for possible fine structure α decays of ^{191m}Po. Events in the rectangles *A*, *B*, *C*, and *D* are discussed further in the text. The inset shows the energy distribution of the α decays from the rectangle *D* of this figure.

^{191m}Po. Moreover, we identified two new groups of α-γ coincidences: 6909(15)-472(1) keV (16 events) and 6790(15)-594(1) keV (2 events). The sum energy balance of these α-γ pairs [and of 6888(5)-494(1) keV events] gives a value of $Q_{\alpha,sum} = Q_\alpha + E_\gamma = 7529(15)$ keV, which is consistent with the $Q_\alpha = 7534(5)$ keV of the 7376 keV transition in ^{191m}Po. This is clearly seen from Fig. 2, where the latter three groups of α-γ events are found on a dashed line, representing the constant value of $Q_{\alpha,sum} = 7534$ keV. Furthermore, from the time distributions between the recoils and corresponding α-γ coincident pairs, the half-life values of 94^{+25}_{-20} ms (6909-472 keV events) and 40^{+90}_{-17} ms (6790-594 keV events) were deduced, in agreement with the half-life of ^{191m}Po. Therefore, on the basis of the α-γ sum energy balance and half-life values we assign the 6909 keV decay and, tentatively, the 6790 keV decay to the fine structure in the α decay of ^{191m}Po.

We would like to provide more information on the origin of the scattered α-γ events in Fig. 2. First of all, the Compton scattering in the Ge detectors produces the low-energy tail of any γ peak: for example, the events in the rectangle *C* (Fig. 2) with $E_\gamma \leqslant 460$ keV, which result from the Compton scattering of the 494 keV γ rays. Furthermore, the α particles, escaping from the PSSD in the backward direction, leave only a part of their energy in the detector. The energy deposition depends on the escaping angle and this effect produced the low-energy tail of any α peak. In Fig. 2 such events are seen, for example, as events with $E_\alpha \leqslant 6800$ keV in coincidence with γ rays at $E_\gamma = 494$ keV. The prompt true coincidences between the escaping α particles and Compton scattered γ rays from the 6888-494 keV group (being the strongest in the spectrum) produce most of the scattered α-γ coincident events in the region of $E_\alpha \leqslant 6800$ keV and $E_\gamma \leqslant 490$ keV.

However, we stress that the two 6790-594 keV events were observed in a practically background-free region with $E_\gamma \geqslant 500$ keV where the amount of possible random coincidences can be reliably estimated by the following simple reasoning. If the two events were random, then one would expect about 40 random α-γ coincidences in the region with $E_\gamma \geqslant 500$ keV for the more intense α decay at 6888 keV. The factor of ≈ 20 is defined by the ratio of the intensities of the 6888 keV and 6790 keV α peaks in the singles α spectrum (Fig. 1). As the α line at 6888 keV has not a single coincidence above $E_\gamma = 500$ keV (Fig. 2), we must conclude that the 6790(15)-594(1) keV coincident events are not random. Despite this, as a result of the low statistics for this decay, we prefer to keep this identification as tentative.

One additional fine-structure α decay of ^{191m}Po was found by analyzing the energy distribution of the α particles in coincidence with the 494 keV γ decay (events in the rectangle *D* of Fig. 2). The inset of Fig. 2 shows the corresponding α-energy spectrum in which, along with a peak at 6888(5) keV, a weaker peak at an *apparent* energy of 6825(15) keV can be seen. As will be shown in the following subsection, the energy (and intensity) of the latter peak must be corrected for the effect of the summing in the PSSD with the energy of electrons, resulting from the strong conversion

of a coincident prompt low-energy γ transition. The corrected energy of 6815(15) keV is shown in Fig. 2. The half-life of $T_{1/2}=91^{+30}_{-20}$ ms for this peak, deduced from the recoil-(α(6825 keV)-γ(494 keV)) correlations, is in agreement with the half-life of the high-spin isomer in ^{191}Po. Based on the Q_α-energy balance, the corrected α-decay energy of 6815(15) keV determines the excitation energy of 573(15) keV for the excited state, fed by this transition.

The decay schemes of both isomers in ^{191}Po are shown in Fig. 3, where for simplicity only the values necessary for discussion are given. Table I gives detailed data on the levels in ^{187}Pb and corresponding feeding α decays of ^{191}Po which will be discussed further in the text.

2. Multipolarities and conversion coefficients for some transitions in ^{187}Pb

The prompt character of all observed α-γ coincidences limits the multipolarity of the corresponding γ transitions to dipole and quadrupole ($\Delta L \leqslant 2$). In some cases a more precise multipolarity determination was possible based on the measured conversion coefficients for these transitions and/or on the hindrance factor (HF) values for the α decays populating the corresponding excited states. Similar to [16], the hindrance factor is defined as the ratio of the reduced α width, calculated by the method of Rasmussen [23], of the transition relative to the reduced α width of the ground-state to ground-state transitions in the neighboring even-even nuclei. As a rule, HF$\leqslant$4 means the same spin, parity, and configuration for the states connected by the α decay [24].

To illustrate our method for deducing conversion coefficients we describe the case of the 6966-375 keV coincidences in more detail. In [16], as a result of low statistics, we were not able to obtain the multipolarity of the 375 keV transition. Figure 4(a) shows the energy spectrum of the γ rays, registered in prompt coincidence with the 6966 keV α line (events in the rectangle *A* of Fig. 2). To reduce the possible contribution from the longer-lived isomer ^{191m}Po to the *K* x-ray region, a time interval of ΔT(recoil-α)$\leqslant$80 ms was additionally applied to produce Fig. 4(a).

The conversion coefficient of the 375 keV transition was deduced by comparing the number of the full energy E_γ

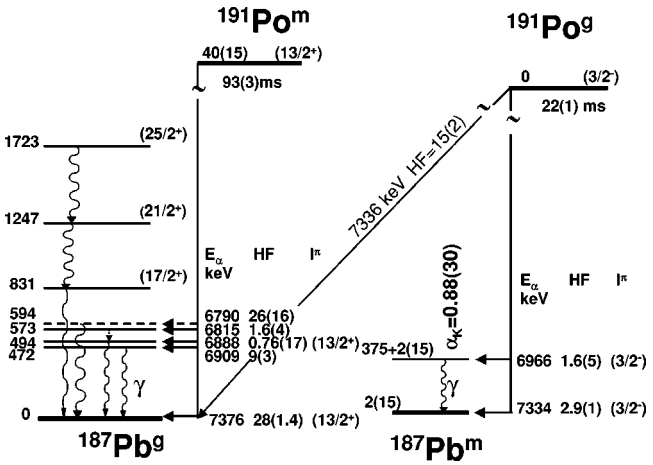

FIG. 3. Alpha-decay scheme of ^{191m,g}Po. For α decays the energies (in keV) and hindrance factors are given. The indicated spin and parity assignments are the values deduced from our analysis. The crossover transition from the low-spin isomer in ^{191}Po to the high-spin isomer in ^{187}Pb is indicated by the slope line. The tentatively identified α decay at 6790 keV and the state at 594 keV are shown by the dashed lines. See main text and Table I for details.

TABLE I. Properties of levels in the high-spin (h.s.) and low-spin (l.s.) isomers of ^{187}Pb. The energies, intensities, and hindrance factors of the feeding α decays of ^{191m,g}Po are shown (column Nos. 2–4). Given uncertainties for the intensities and hindrance factor values include both statistical errors and $\approx$20% uncertainty in the γ efficiency for the values, deduced from the α-γ coincidence data. Energies of the γ rays, deexciting the level, and corresponding experimental and calculated conversion coefficients [26] are given in column Nos. 5–9. Spin and parity assignments which are possible on the basis of experimental data only are given in column No. 10 (possible I^π), while the final assignments are shown in the last column. Tentative I^π assignments are shown in brackets.

Level (keV)	Feeding α decay (keV)	I_α (%)	HF	E_γ (keV)	α_K (Expt.)	α_K $E1$	α_K $E2$	α_K $M1$	Possible I^π	I^π Assigned
^{187}Pb(h.s.)										
0	7376(5)[a]	47.6(1.5)	28(1.5)							$13/2^+$
0	7336(15)[b]	15(2)	15(2)							
472(1)	6909(15)[a]	3.9(1.1)	9(3)	472(1)	$\leqslant$0.06	0.009	0.024	0.11	$9/2^+$-$17/2^+$	$(9/2^+)$
494(1)	6888(5)[a]	38(8)	0.76(17)	494(1)	0.076(20)	0.008	0.021	0.095	$11/2^+$-$15/2^+$	$(13/2^+)$
573(15)	6815(15)[a]	10(2)	1.6(4)	80(15)[c]	$\geqslant$10[d]	0.12[d]	17[d]	3.41[d]	$9/2^+$-$17/2^+$	$(9/2^+)$
594(1)[e]	6790(15)[a]	0.5(3)	26(16)	594(1)						
^{187}Pb(l.s.)										
2(15)	7334(5)[b]	77.0(2.5)	2.9(1)							$3/2^-$
375(1)+2(15)	6966(10)[b]	8.0(2.3)	1.6(5)	375(1)	0.88(30)	0.014	0.04	0.2	$3/2^-$	$3/2^-$

[a]From ^{191m}Po(h.s.).

[b]From ^{191g}Po(l.s.).

[c]Unobserved, presumably strongly converted, transition.

[d]Total conversion coefficients.

[e]Tentatively assigned on the basis of two α-γ coincident events only.

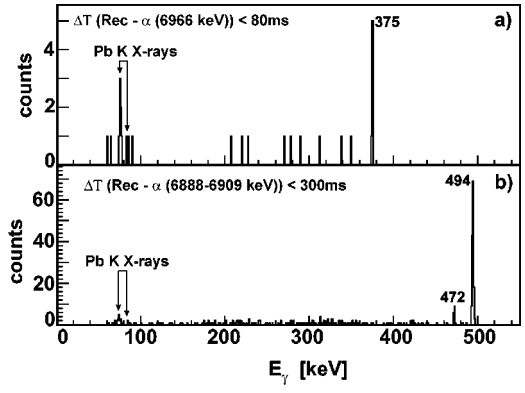

FIG. 4. (a) Prompt γ-ray spectrum from recoil-α-γ coincidences for the 6966 keV line of ^{191g}Po (events from rectangle *A* of Fig. 2). (b) The same, but in coincidence with the 6888 α line of ^{191m}Po (events from the rectangle *C* of Fig. 2). The recoil-α correlation time intervals were 80 ms and 300 ms, respectively.

$=375$ keV events with the number of *K* x rays in Fig. 4(a) after normalization for the corresponding γ and *K* x-ray efficiencies. Furthermore, this value must be corrected for the effect of full and/or partial summing in the PSSD of the α-particle energy (6966 keV) with the energy of the conversion electron, $E_{e^-}=375-88$ keV$=287$ keV (88 keV being the binding energy of the electron in the *K* shell of the daughter lead nuclei), giving a total energy of ≈ 7253 keV. Such summing effects have been discussed in detail in [19] and calculations, carried out using the GEANT Monte Carlo code [25], confirm that the thickness of the PSSD is enough to stop most of such electrons when they are emitted in the PSSD. An α line with an energy of 7254(20) keV was indeed observed both in the singles α spectrum (see inset in Fig. 1) and in the prompt α-γ matrix as a group of 7254(20) keV-*K* x-ray coincidences (see Fig. 2, rectangle *B*). The time behavior of these events, deduced from recoil-α(7254 keV)-*K* x-ray analysis, is consistent with the half-life of the 7334 keV α line. Therefore, we interpret the 7254(20) keV line as an artificial one, resulted from the full-energy α-e^- summing.

In our previous study such a line with rather low statistics was also observed in the α spectrum (see Fig. 1 of Ref. [16]) and was tentatively assigned as a crossover transition from the low-spin isomer of ^{191}Po to the high-spin isomer in ^{187}Pb (dashed line in Fig. 2 of [16]). However, the improved statistics along with the $\alpha-$x-rays coincidences for this line rule out this assignment.

If the conversion electron escapes from the Si detector in the backward direction, a variable amount of its energy, depending on the escaping angle, will be summed up with the energy of the coincident α decay. This effect produces, for example, the high-energy tail of the α line, which is seen in Fig. 2 as the events along the vertical line, extending from the α(6966 keV)-*K* x-ray group up to the α(7254 keV)-*K* x-ray group.

There could be a contribution to the discussed groups of α-e^--*K* x rays events from the conversion and subsequent summing of the electrons from the 494 keV γ line in coincidence with the 6888 keV α decay of ^{191m}Po. This contribution was estimated and subtracted by producing a prompt α-γ matrix similar to Fig. 2, but for a recoil-α time interval of 80–240 ms, which indeed shows the events from the longer-lived nucleus ^{191m}Po only. Finally, by comparing the number of 6966-375 keV events on the one hand and of background-subtracted 6966 keV-*K* x rays or/and 7254 keV-*K* x rays on the other, after correcting for the corresponding measured γ, *K* x-ray efficiencies and calculated α-e^- summing efficiencies, a conversion coefficient of $\alpha_K=0.88(30)$ was deduced for the 375 keV γ transition. This value is only compatible with the theoretical conversion coefficient of $\alpha_K(M2)=0.61$, while $\alpha_K(M1)=0.2$, and $\alpha_K(E1)$ and $\alpha_K(E2)$ are at least one order of magnitude lower [26]. However, the parity-changing $M2$ multipolarity should be ruled out as it would conflict with rather similar hindrance factors for the 7334 keV (HF$=2.9$) and the 6966 keV (HF $=1.6$) α transitions feeding the two levels connected by the 375 keV γ decay. All this results in a mixed $E0$-$M1$-$E2$ multipolarity assignment to the 375 keV transition in order to explain its high conversion coefficient.

The low hindrance factors of the 7334 keV and 6966 keV α transitions and the $E0$ component in the 375 keV γ transition yield the same spin and parity for the three levels connected by these three transitions. As a $3/2^-$ assignment for the low-spin isomer in ^{187}Pb is favored by systematics, the spin and parity for the low-spin isomer in ^{191}Po and of the 375 keV level in ^{187}Pb are also $3/2^-$.

Figure 4(b) shows the energy spectrum of the γ rays, registered in prompt coincidence with the 6888 keV α decay (events in the rectangle *C* of Fig. 2), populating the excited state at 494 keV in the high-spin isomer of ^{187}Pb. The recoil-α correlation time was 300 ms. In [16] we suggested an $E0$ component in the decay of this level which was interpreted as an intruder state, resulting from the coupling of the $1i_{13/2}$ neutron to the $\pi(2\text{p-}2\text{h})$ oblate intruder state in the neighboring even lead core. In the current study by comparing the number of full energy $E_\gamma=494$ keV events with the number of *K* x rays in Fig. 4(b) after correcting for the corresponding efficiencies and taking into account α-e^- summation effects similar to the case of the 375 keV transition, a conversion coefficient of $\alpha_K=0.076(20)$ can be deduced for the 494 keV γ transition. This value should be compared with the theoretical conversion coefficients of $\alpha_K(E2)=0.021$ and $\alpha_K(M1)=0.095$, while other possibilities can be excluded [$\alpha_K(E1)=0.008$ and $\alpha_K(M2)=0.264$; see Table I]. This suggests the 494 keV transition to be a pure $M1$ transition or a mixture of $E0$-$M1$-$E2$ transitions, thus establishing a range of possible spin and parity values for the excited state at 494 keV as $11/2^+$-$13/2^+$-$15/2^+$. From the low hindrance factor (HF$=0.76$) for the 6888 keV α decay of ^{191m}Po one can conclude that the spin and parity of the high-spin isomer in ^{191}Po and of the 494 keV state in the high-spin isomer in ^{187}Pb are the same. This also leads to a series ($11/2^+$-$13/2^+$-$15/2^+$) of possible candidates for the spin and parity of ^{191m}Po. Anticipating the detailed discussion in Sec. IV we note that the potential-energy surface calculations and particle-plus-rotor calculations suggest that the most prob-

able spin and parity for ^{191m}Po and for the 494 keV excited state in the high-spin isomer in ^{187}Pb are $13/2^+$.

We would like to comment on the suggested $E0$ component in the 494 keV γ decay [16]. As shown above, in the present study the evidence for an $E0$ component in this decay was found to be rather weak. The presence of an $E0$ component in the 494 keV transition was deduced in [16] from the prompt α-γ matrix (see Fig. 2 of [16]) by comparing the number of α(6888 keV)-γ(494 keV) coincident pairs with the number of α(6888)-K x-ray and $[\alpha(6888\ \text{keV})+e^-]$-$K$ x-ray coincident events. However, in [16] as a result of lower statistics, the half-life analysis and background estimation in the α(6888 keV)-K x-ray and $[\alpha(6888\ \text{keV})+e^-]$-$K$ x-ray regions, similar to described above for the $[\alpha(6966\ \text{keV})+e^-]$-$K$ x-ray events, could not be done. All this resulted in an overestimated number of the α-K x-ray and $[\alpha+e^-]$-K x-ray events when deducing the conversion coefficient for the 494 keV γ transition.

The deduced conversion coefficient for the 494 keV transition should in principle be considered as an upper limit, as the 472 keV γ line in coincidence with the 6909 keV α decay of ^{191m}Po is also present in Fig. 4(b) and its possible internal conversion could give a surplus of events in the region of the K x-ray, corresponding to the 494 keV line. However, based on careful analysis of the α-energy distributions from the 6909-472 keV and 6888-494 keV coincident pairs on the one hand and of 6909-K x rays and 6888-K x rays on the other hand, we conclude that the contribution of K x rays from the possible internal conversion of the 472 keV γ decay is negligible and will not influence our conclusion on the multipolarity of the 494 keV γ decay. An upper limit for the measured conversion coefficient for the 472 keV γ line is $\alpha_K \leqslant 0.06$, which is consistent with $E2$ [α_K(theor) $=0.024$] or $E1$ [α_K(theor)$=0.009$] multipolarity assignments. This suggests a possible spin and parity of this state in the range of $11/2^-$-$15/2^-$ ($E1$) or $9/2^+$-$17/2^+$ ($E2$) based on the $I^\pi = 13/2^+$ assignment for the high-spin isomer in ^{187}Pb. The tentative I^π and configuration assignments for this state were further done on the basis of HF values and particle-rotor calculations, discussed in Sec. IV.

A spin and parity estimate can be also given to the state at 573(15) keV, populated by the 6815(15) keV α decay (see Fig. 3). As was mentioned above, the observed *apparent* energy of this decay is, in fact, about 6825(15) keV (see inset to Fig. 2). This would define the energy of the excited state, fed by this decay, as 563(15) keV, thus about 70(15) keV above the 494 keV state. The former state must promptly decay to the latter one as the 6825(15) keV decay is observed in prompt coincidences with the 494 keV transition. As a result of relatively low statistics and the presence of some scattered events in the region of low-energy γ rays, we can give only an upper limit of $\leqslant 9$ counts for the number of 6825(15)-70(15) keV decays (see Fig. 2). However, the expected intensity of the latter decay can be reliably calculated based on the observed number of the 6825-494 keV decays as the two γ decays proceed in a cascade. By comparing the above-given upper limit and calculated intensity, normalized on the corresponding γ-ray efficiencies and conversion coefficient of the 494 keV decay, a lower limit of $\alpha(\text{tot}) \geqslant 4$ for the total conversion coefficient of the low-energy transition can be given. As a result of a rather high conversion coefficient and subsequent α-e^- summing in the Si detector, a correction must be done of the measured α-decay energy and intensity for the 6825 keV transition. According to GEANT calculations, this effect shifts the α peak to higher energies by about 10 keV and produces a higher-energy peak, similar to the case of the 375 keV decay, discussed above. By taking these effects into account the absolute intensity of 10(2)%, the unshifted energy of 6815(15) keV and the hindrance factor value of HF$=1.6(4)$ were deduced for this α decay. This establishes the excitation energy of 573(15) keV for the state, fed by this decay (see Fig. 3), thus about 80(15) keV relative to the $13/2^+$ oblate bandhead at 494 keV.

Based on the deduced intensity for the feeding 6815 keV decay, a corrected lower limit of $\alpha(\text{tot}) \geqslant 10$ was deduced for the total conversion coefficient of the 80(15) keV decay. This value suggests a rather pure $E2$ multipolarity for this transition, as theoretical total conversion coefficients are $\alpha(\text{tot}, M1) = 3.4$ and $\alpha(\text{tot}, E2) = 17$ [26]. Higher multipolarities must be excluded as they would contradict with the prompt character of this transition. This defines a possible spin and parity of this state in the range of $9/2^+$-$17/2^+$ based on the $13/2^+$ spin and parity for the 494 keV state in ^{187}Pb.

The multipolarity of the tentatively assigned 594 keV transition in the high-spin isomer in ^{187}Pb could not be determined due to the low statistics.

3. Crossover $^{191}Po(l.s.) \rightarrow {}^{187}Pb(h.s.)$ α decay

A search was undertaken for the crossover transitions between the $3/2^-$ low-spin isomer in ^{191}Po and the $13/2^+$ high-spin isomer of ^{187}Pb [^{191}Po(l.s.)$\rightarrow{}^{187}$Pb(h.s.) α decay] as well as between the $13/2^+$ high-spin isomeric state of ^{191}Po and the $3/2^-$ low-spin isomer of ^{187}Pb [^{191}Po(h.s.) $\rightarrow{}^{187}$Pb(l.s.) α decay]. The excitation energy of the $13/2^+$ isomeric state relative to the $3/2^-$ (^{197,199,201}Po) or $5/2^-$ (^{203,205,207}Po) ground state in the heavier odd-mass nuclei [4] decreases from ≈ 1100 keV in ^{207}Po down to ≈ 200 keV in ^{197}Po. A similar trend exists for the $13/2^+$ and $3/2^-$ isomeric states in the odd-mass lead nuclei. For example, in ^{193}Pb the $13/2^+$ isomeric state was estimated to be only about 100 keV above the $3/2^-$ ground state [4]. In the lighter lead nuclei one expects a crossing of the $13/2^+$ and $3/2^-$ isomeric states. Therefore it is expected that the energies of crossover α decays should not be very different from the highest-energy 7334 keV and 7376 keV α decays of ^{191}Po.

According to hindrance factor calculations using the method of Rasmussen [23], both crossover decays should be retarded by a factor of 15 due to $\Delta L = 5$ angular momentum change if there is no additional hindrance due to possible structure changes. One expects therefore to observe such crossover transitions with intensities of about 700 counts since the intensities of the 7334 and 7376 keV α lines of ^{191}Po are about 11 000 α particles each. However, in the singles α spectrum (inset to Fig. 1) no additional peaks with the expected intensity can be seen. This suggests that either there is a much stronger hindrance factor due to additional

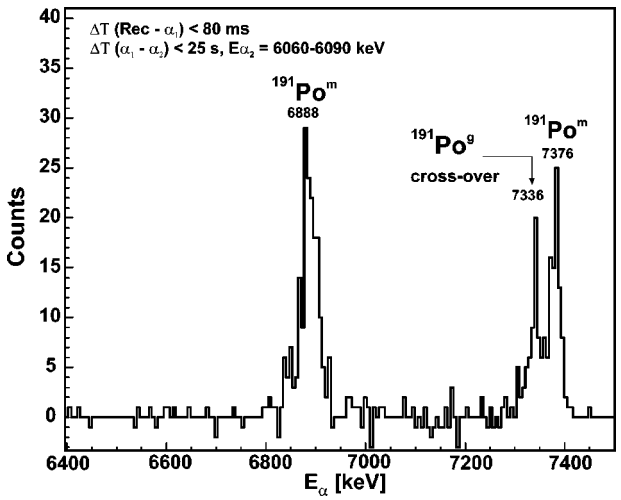

FIG. 5. Background-subtracted α_1 spectrum from recoil-α_1-α_2(6070 keV,^{187}Pb(h.s.)) correlations with a gate on the α decay of the daughter nucleus ^{187}Pb(h.s.). See main text for details.

structure changes or the energies of the crossover transitions are indeed very similar to the 7334 keV and 7376 keV α decays and are masked by these much stronger $\Delta L=0$ decays.

Hence, to make a more sensitive search, we undertook a recoil-α_1-α_2 correlation analysis. To enhance the observation of the crossover transition between the $3/2^-$ state of ^{191}Po ($T_{1/2}=22$ ms) and the lowest $13/2^+$ state of ^{187}Pb a time interval of ΔT(recoil-α_1)$=0-80$ ms was used. The parameters for the α_2 decay ($\Delta T(\alpha_1$-$\alpha_2)=0-25$ s,$E_{\alpha_2}=6060-6090$ keV) were chosen to observe the 6070 keV α decay of the high-spin isomer in the daughter ^{187}Pb ($T_{1/2}=18$ s). Note that a relatively narrow interval for the α_2 decay was applied to avoid the contribution from the α-e^- summing of the 5993 keV decay and the conversion electrons of ≈ 53 keV from the strongly converted 67 keV decay [27]. Unfortunately, despite the low implantation rate and the high effective number of pixels in the PSSD, a rather long time for the α_1-α_2 correlations resulted in some random events. This was taken into account by producing a spectrum of random α_1 decays from recoil-α_1-α_2(^{191}Po(h.s.)) "self-correlations." Here we applied the same time intervals for the α_1 and α_2 decays as in the above case, but with an energy gate of 6880–6900 keV on the α_2 decay, which corresponds to the fine-structure α decay of the high-spin isomer in ^{191}Po.

The two α_1 spectra were then normalized to the same number of random recoil-α_1(^{192}Po)-α_2 correlations for the ^{192}Po nucleus ($E_\alpha=7167$ keV; see Fig. 1) which in both cases does not have real correlations within the chosen energy interval for the α_2 decay. The difference of these two spectra is shown in Fig. 5. Only three peaks with energies of 6888(10) keV, 7336(15) keV, and 7376(10) keV can be clearly seen in this spectrum. The 6888 keV and 7376 keV α peaks represent the ^{191}Po(h.s.)$\rightarrow$^{187}Pb(h.s.) decays of the $13/2^+$ isomeric state in ^{191}Po towards the excited and the lowest $13/2^+$ states in ^{187}Pb, correspondingly. By comparing the number of the recoil-α_1(7376 keV) and recoil-α_1(7376 keV)-α_2(6070 keV,^{187}Pb(h.s.)) correlations a branching ratio of $\alpha_{br}=12(2)\%$ for the high-spin isomer in ^{187}Pb can be deduced in agreement with [16].

The peak at 7336(15) keV in Fig. 5, although having practically the same energy as the 7334(5) keV line from the ^{191}Po(l.s.)$\rightarrow$^{187}Pb(l.s.) decay, can be only explained as a crossover transition between the low-spin $3/2^-$ isomeric state in ^{191}Po and the high-spin $13/2^+$ isomeric state in ^{187}Pb. Also the half-life of this line [$T_{1/2}$(7336 keV) $=25(6)$ ms] is consistent with the half-life value of ^{191g}Po. Based on the deduced branching ratio of the high-spin isomer in ^{187}Pb and on the number of observed 7336 keV events in Fig. 5, one can deduce a total number of 7336 keV crossover decays originating from the low-spin isomer in ^{191}Po. This value, together with the intensities of the 6966 keV and 7334 keV α decays of the low-spin isomer in ^{191}Po, defines the branching ratio and hindrance factor values for these decays as shown in Fig. 3. The hindrance factor value of HF$=15(2)$ for the 7336 keV crossover transition is in good agreement with the calculated hindrance factor of 15 for a $\Delta L=5$ transition.

This crossover transition establishes the excitation energies of the $13/2^+$ and $3/2^-$ states relative to each other in ^{191}Po and in its daughter ^{187}Pb and granddaughter ^{183}Hg nuclei. In agreement with the systematics of the heavier odd-mass Po nuclei, the $13/2^+$ isomeric state is still above the $3/2^-$ ground state in ^{191}Po, but it continues its downward behavior, lying only 40(15) keV higher than the $3/2^-$ ground state. Within the experimental accuracy on the α-energy determination the positions of the $13/2^+$ and $3/2^-$ states are reversed in ^{187}Pb, the $13/2^+$ state becoming the ground state with the $3/2^-$ state lying only 2(15) keV above it. That is why, in Fig. 3, the high-spin and the low-spin states in ^{187}Pb are denoted as the ground state and isomeric state, correspondingly. In the granddaughter ^{183}Hg the high-spin (presumably $13/2^+$) isomeric state has an excitation energy of 191(20) keV, relative to the $1/2^-$ ground state.

The 7336(15) keV crossover decay ^{191}Po(l.s.) $\rightarrow$^{187}Pb(h.s.) establishes the energy for the possible ^{191}Po(h.s.)$\rightarrow$^{187}Pb(l.s.) crossover decay at 7374(15) keV. Following the same procedure as in the case of the 7336 keV decay, a recoil-α_1-α_2(^{187}Pb(l.s.)) correlation analysis was performed. The daughter ^{187}Pb(l.s.) nucleus has a half-life of 15 s and decays by two α branches with $E_\alpha=5993$ keV and $E_\alpha=6194$ keV [4,16,27]. Search time intervals of ΔT(recoil-α_1)$=0-400$ ms, $\Delta T(\alpha_1$-$\alpha_2)=0-25$ s, and an energy gate of 6170–6260 keV on the daughter α_2(^{187}Pb(l.s.)) decay were used. The broader gate on the α_2 energy is caused by the energy summing of the 6194 keV α line with conversion electrons from the highly converted 67 keV transition in ^{183g}Hg fed by this α decay [27]. In the resulting background-subtracted spectrum, similar to Fig. 5, we clearly observe the 6966 keV and 7334 keV α decays of ^{191g}Po. By comparing the numbers of the recoil-α_1(7334 keV) and recoil-α_1(7334 keV)-α_2(^{187}Pb(l.s.)) correlations a branching ratio of $\alpha_{br}=9.5(2.0)\%$ for ^{187}Pb(l.s.) can be deduced. This value is slightly higher than

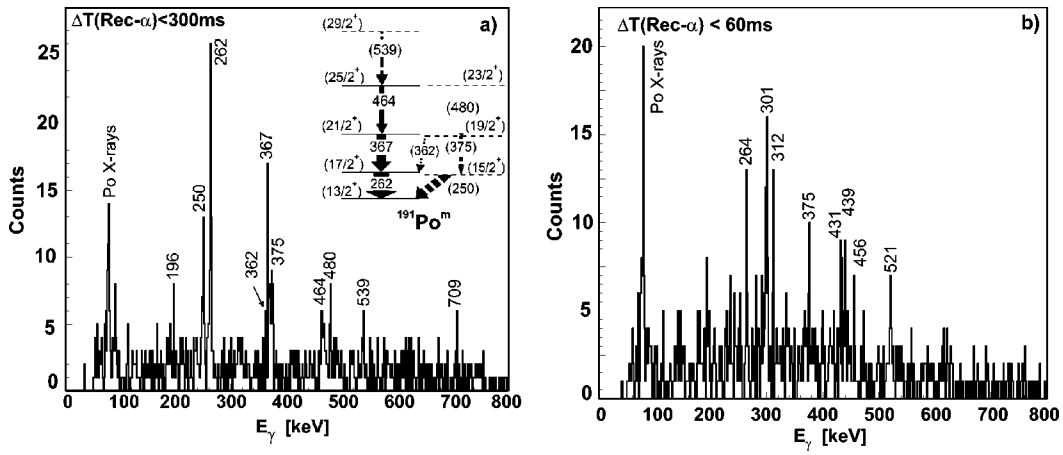

FIG. 6. Prompt singles γ-ray spectra tagged with the 7376 keV α decay of ^{191m}Po (a) and with the 7334 keV α decay of ^{191g}Po (b). Inset to (a) shows the deduced level scheme built on top of the $13/2^+$ state. Energies are given in keV. Tentative levels are shown by dashed lines.

$\alpha_{br}=7(2)\%$ from [16] since in the previous study the 7336 keV crossover transition was not known and therefore not taken into account.

At the expected position of the crossover transition at 7374 keV a weak peak with a few counts only was observed, this potentially corresponds to the ^{191}Po(h.s.)$\rightarrow{}^{187}$Pb(l.s.) crossover decay. However, we cannot fully exclude that this weak peak results from incomplete background subtraction. Therefore, using this number as an upper limit and based on the obtained branching ratio of ^{187}Pb(l.s.), a hindrance factor value of HF$\geqslant$80(20) can be deduced for the possible 7374 keV crossover decay. The higher hindrance factor for this transition, compared to the 7336 keV crossover transition, can be presumably related to additional hindrance due to structure change between the states, connected by this decay as will be discussed in Sec. IV.

We note that as a result of the large hindrance factor for the possible 7374 keV crossover decay, the corresponding correction for the number of recoil-α_1(^{191m}Po) decays when deducing the α-branching ratio of ^{187g}Pb is very small and in practice does not change the final value.

B. Excited states in ^{191m,g}Po

Before this experiment no excited states were reported for ^{191m,g}Po. Prompt γ spectra, collected by the Jurosphere Ge detectors and gated by the 7376 keV and 7334 keV α decays of ^{191}Po, are shown in Figs. 6(a) and 6(b), respectively. To reduce the random coincidences, time windows of 300 ms and 60 ms between recoil implantation and corresponding α decay were applied to produce the spectra in Figs. 6(a) and in 6(b), respectively. In Fig. 6(a), along with the Po K x rays, the following main γ peaks can be distinguished: 196 keV, 250 keV, 262 keV, 362 keV, 367 keV, 375 keV, 464 keV, 480 keV, 539 keV, and 709 keV. Based on the observed γ-ray intensities and on the extensive level systematics for the heavier odd-mass Po nuclei [10] the γ rays can be tentatively grouped in two sequences of transitions; see inset to Fig. 6(a). The first sequence establishes the 262 keV $(17/2^+)$-629 keV$(21/2^+)$-1093 keV$(25/2^+)$-1632 keV $(29/2^+)$ states, which are interpreted as the favored states, built on top of the $13/2^+$ isomeric state, as is observed in all heavier odd-mass Po nuclei up to $A=207$. This assignment is further confirmed by the observation of mutually coincident prompt recoil-gated γ-γ events between the 262 keV, 367 keV, and 464 keV γ rays. In particular, two recoil-262-367 keV coincidence events and one recoil-262-464 keV coincidence event have been found along with one recoil-367-464 keV coincidence event. The second sequence of 250 keV$(15/2^+)$-625 keV$(19/2^+)$-1105 keV$(23/2^+)$ states was tentatively assigned to the unfavored states of the same band. This assignment, like in the case of ^{193,195}Po where such unfavored states were also observed [10], is based on the energy sums and intensities of the corresponding γ rays. Unfortunately, as a result of low statistics, no γ-γ coincident events have been observed for this band. The states for which no coincidences could be established, presumably because of low statistics, are shown by the dashed lines.

A few γ transitions have been observed on top of the $3/2^-$ state of ^{191}Po [Fig. 6(b)], but as a result of low statistics and lack of coincidences, the construction of a level scheme was not possible. This is also the case for the $3/2^-$ isomer in ^{193,195}Po, where a few γ transitions were observed, but could not be placed due to low statistics. Note that the strong Po K x rays, observed in Fig. 6(b), suggest the presence of converted relatively low-energy transitions in the low-spin isomer.

The 196 keV and 709 keV γ peaks, seen in Fig. 6(a), but not in Fig. 6(b), should originate from the high-spin isomer in ^{191}Po, but could not be placed in the decay scheme due to lack of coincidences.

To conclude this section, we stress a clear difference between the patterns of the excited states observed on top of the two isomeric states in ^{191}Po. A clear rotationlike structure in the high-spin isomer is an indication of its more deformed shape, while a more fragmented pattern in the low-spin isomer points to its weakly deformed or near-spherical shape.

Further discussion of the energy systematics of the excited states in the odd-mass Po nuclei will be given in Sec. IV C.

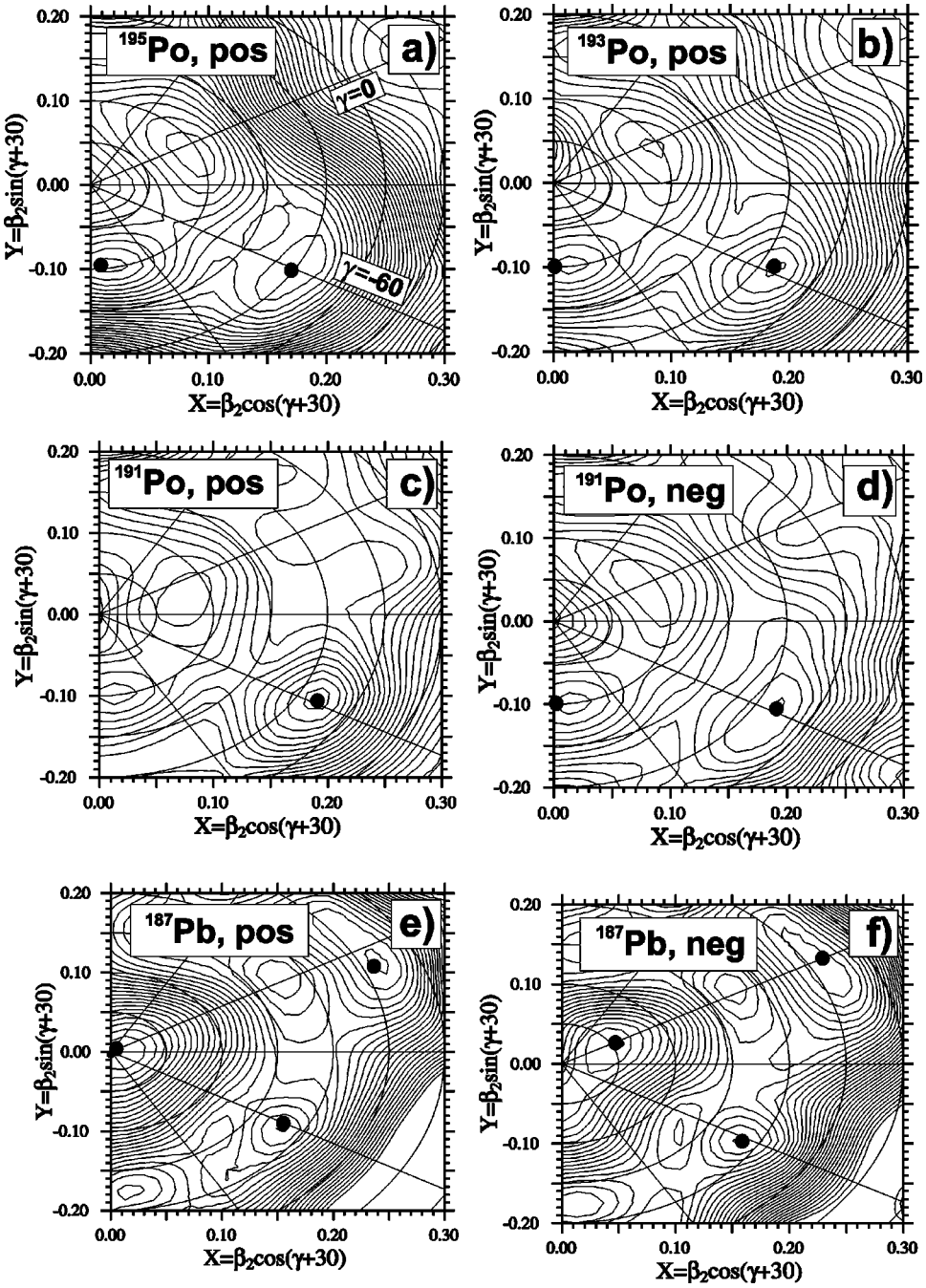

FIG. 7. Total potential-energy surfaces for ^{195m}Po (a), ^{193m}Po (b), ^{191m}Po (c), ^{191g}Po (d), ^{187}Pb (h.s.) (e), and ^{187}Pb (l.s.) (f). Different minima are indicated by black dots. The energy distance between contour lines is 50 keV [except for (c) and (d), 100 keV]. The $\gamma=0$ corresponds to prolate (cigarlike) shape and $\gamma=-60$ to oblate (disklike) shape.

IV. DISCUSSION

A. Potential-energy surface calculations and particle-plus-rotor calculations for the odd-mass lead and polonium nuclei with $A \leqslant 195$

In the previous section we presented experimental data on low-spin and high-spin states in ^{191}Po and its daughter ^{187}Pb. Mainly as a result of low statistics, the unique spin and parity assignment to some states was not possible.

In an attempt to make more precise assignments and to shed more light on the structure of the different states in these and in other very-neutron-deficient lead and polonium nuclei we performed potential-energy surface calculations and particle-plus-rotor calculations. The PES calculations are based on the Strutinsky shell correction approach [28]. The single-particle energies are obtained from the deformed Woods-Saxon potential with universal parameters [29]. Pairing correlations are treated by means of a seniority and double-stretched quadrupole pairing force with approximate particle number projection according to the Lipkin-Nogami scheme [30]. The odd-particle configurations are blocked fully self-consistently in the calculations. For more details of the method we refer the reader to Ref. [31].

Different minima in the potential-energy surface, corresponding to coexisting spherical, prolate, and oblate configurations, are predicted for very-neutron-deficient lead and polonium nuclei. As an example, Fig. 7 shows the results of potential-energy surface calculations for the positive parity

states in ^{193,195}Po and for the positive and negative parity states in ^{187}Pb and ^{191}Po.

For the particle-plus-rotor (PPR) calculations we used the same Woods-Saxon potential as for the PES calculations. The minima of the PES calculations define the quadrupole, hexadecapole, and triaxiality deformation parameters β_2, β_4, and γ for each coexisting configuration, these values in turn determining the single-particle spectrum of the PPR calculations. The only additional input is the 0^+-2^+ core energy for each deformed minimum, which determines the moment of inertia and hence the strength of the Coriolis interaction. The *unperturbed* 0^+-2^+ energies were obtained from spectra of excited states in the neighboring even-even nuclei. Since the oblate band is not known in ^{186,188}Pb [32,33], to deduce the parameters for the oblate band in ^{187}Pb we used the energy difference between the *unperturbed* 0^+ and 2^+ states of oblate bands recently identified in ^{192,194}Po (see details in [10]). To estimate the unperturbed 0^+-2^+ energy in the prolate minimum, the known prolate bands in ^{184,186,188}Pb have been used (see discussion in [34]). The PPR calculations can be viewed as a way to project the proper single-particle spectrum present at the deformed minimum. No Coriolis attenuation factor has been applied and with the parameters used we could reproduce the behavior of the oblate rotational bands based on the $1i_{13/2}$ neutron in the neutron-deficient odd-mass Hg isotopes. However, we mention that as a result of limited experimental information on such oblate bands, especially in the vicinity of the midshell at $N=104$, the adjustment of Coriolis interaction parameters is somewhat uncertain. With this approach we expect to have the bandhead spin assignment correct although the calculated energy spacing (moment of inertia) will be more compressed than the measured values. The combination of the PPR and PES calculations is discussed in detail in Refs. [35] and [36].

Finally, we remark on an important aspect when dealing with the energies of different minima extracted from PES calculations and their comparison to experimental values. PES calculations give the mean-field value of the energy at the lowest point in the surface. The coupling to the vibrational motion, including zero-point motion, is not taken into account. These ground-state correlations can be approximated by means of the random phase approximation(RPA) or the generator-coordinate method [37]. Both methods result in a lowering of the ground-state energy. Hence, the discrepancy between results of PES calculations and experimental data may reflect limitations in the method and not necessarily the deficiency of the parameters of the mean-field potential. We expect these correlations to depend on the shape of the nucleus and also to be more important in even-even nuclei. At spherical shapes the presence of low-lying collective states will result in an enhancement of ground-state correlations. On the other hand, the transition from a soft spherical potential-energy surface to one in which three coexisting minima are present will most likely reduce the correlation energy at the spherical minimum.

B. Configuration, spin, and parity assignment of the α-decaying states in ^{191}Po

1. Positive parity states

According to PES calculations the structure of the positive parity states in the odd-mass Pb and Po nuclei close to the neutron midshell at $N=104$ is associated with the neutron $i_{13/2}$ configuration.

A nearly spherical $(\beta_2=0.1,\gamma=-120)$ $\nu 1i_{13/2}\otimes\pi(2\text{p-}0\text{h})$ configuration is predicted to be the lowest in energy for the positive parity states in ^{193m,195m}Po; see Figs. 7(a) and 7(b). The slightly deformed shape of these nuclei reflects the driving property of the proton pair in the strongly downsloping $h_{9/2}$-$f_{7/2}$ Nilsson orbitals [1]. It is difficult to speak of well-defined shapes, but the structure of the Po nuclei differs from the one of the daughter Pb isotopes, especially in the presence of an odd particle.

A rather shallow oblately deformed coexisting minimum $(\beta_2=0.22,\gamma=-60)$ at an excitation energy of about 600 keV is present in ^{195}Po [Fig. 7(a)]. In the particle-hole picture this minimum can be explained by the interaction of the deformed intruder $\pi(4\text{p-}2\text{h})$ configuration (oblate state) with the valence neutrons, in particular from the $1i_{13/2}$ orbital. By decreasing the neutron number this configuration lowers its energy and in ^{193}Po the oblate state is predicted at an excitation energy of 100–200 keV only, relative to the spherical one [Fig. 7(b)]. As will be shown in Sec. IV B 3, in both nuclei these two configurations are somewhat mixed, which is clearly seen from the α-decay data.

In ^{191}Po the situation is completely different as a single well-defined oblate minimum with $\beta_2=0.22$ and $\gamma=-60$ [see Fig. 7(c)] is predicted by calculations, while the rather shallow nearly spherical configuration is now higher in energy. Based on the α-decay data we will show below that there is practically no mixing between the two coexisting configurations in ^{191}Po (h.s.).

In ^{187}Pb (h.s.) in addition to a dominant spherical minimum due to the shell closure at $Z=82$, two coexisting minima at $\beta_2\approx 0.2$ and $\gamma=-60$ (oblate) and at $\beta_2\approx 0.25$ and $\gamma\approx 0$ (prolate) are predicted; see Fig. 7(e).

In order to predict the spin and parity of the bandhead states in the oblate minimum of ^{187}Pb(h.s.) and ^{191}Po(h.s.) PPR calculations have been performed. By comparing Figs. 7(c) and 7(e), one sees that PES calculations predict similar parameters (β_2, β_4, and γ) for the oblate minimum in these nuclei. At oblate deformation for positive parity states we deal essentially with the unique parity $1i_{13/2}$ orbital. In the absence of (or with weak) Coriolis interaction one would expect the lowest state of positive parity to reflect the change in neutron number and, hence, in the Ω value of the odd particle.

However, the strong Coriolis interaction at oblate shapes (small moments of inertia, large j value, and the narrow distance between the levels of the $i_{13/2}$ subshell) results in a lowering of the $13/2^+$ state. With no Coriolis attenuation used, the $13/2^+$ state is predicted to be the lowest in energy in the oblate minimum from the top of the shell up to

$N=103$, in which the oblate minimum practically disappears in the PES calculations. In this case, at $N=105$ (^{187}Pb), the following sequence of the states is predicted above the $13/2^+$ oblate bandhead: $11/2^+$ at 10 keV, $9/2^+$ at 50 keV, $15/2^+$ at 170 keV. This weakens the possibility of the $11/2^+$ or $15/2^+$ assignments to the oblate band head states in the high-spin isomers of ^{187}Pb and ^{191}Po, which could be possible on the basis of the conversion coefficient measurements (see Table I and Sec. III A 2).

The $I^\pi=13/2^+$ assignment to the α-decaying state in ^{191}Po(h.s.) is put on a stronger footing by taking into account the α-decay pattern. By considering the Nilsson orbitals involved in building up the oblate states in this case, the main configurations are $\nu 1i_{13/2}\otimes\pi(4p\text{-}2h)$ in ^{191}Po and $\nu 1i_{13/2}\otimes\pi(2p\text{-}2h)$ in ^{187}Pb. In this case an unhindered α decay is expected to proceed by removing a proton pair from above the $Z=82$ shell gap together with one of the valence neutron pairs. The excited state at 494 keV in ^{187}Pb(h.s.) is a candidate for this configuration as it is fed by unhindered (HF=0.76,$E_\alpha=6888$ keV) α decay. The α decay to the spherical $\nu 1i_{13/2}\otimes\pi(0\text{p-}0\text{h})$ ground state in ^{187}Pb(h.s.) should be hindered, despite its $\Delta L=0$ character, as it involves a two-step process: removal of a proton pair above the $Z=82$ shell gap and deexcitation of a proton pair from above to below the gap. This is indeed seen experimentally: the decay towards the lowest $13/2^+$ state in ^{187}Pb is about 37 times slower compared to the decay towards the $13/2^+$ intruder state at 494 keV. This means that the $13/2^+$ isomeric state in ^{191}Po is a pure intruder $\pi(4p\text{-}2h)$ oblate configuration and its mixing with the normal $\pi(2p\text{-}0h)$ spherical configuration is very small.

2. Negative parity states

The situation is different for the negative parity states in ^{191}Po. According to PES calculations the negative parity states have a nearly spherical gamma-soft minimum with $\beta_2=0.1,\gamma=-120$ coexisting with a rather shallow oblate minimum with $\beta_2=0.22,\gamma=-60$ at an excitation energy of about $\approx$100–200 keV; see Fig. 7(d). In the particle-hole picture these minima can be explained by the interaction of the $\pi(2\text{p-}0\text{h})$ configuration (near-spherical state) or the $\pi(4\text{p-}2\text{h})$ configuration (oblate state) with the valence neutrons, in particular from the $3p_{3/2}$ and $2f_{5/2}$ orbitals. Note, however, the difference in shape and softness of the near-spherical minimum for negative and positive parity states. The results of the PPR calculations for the negative parity states in the near-spherical minimum are not as well determined as in the case of the positive parity states. This is partly due to the fact that for the near-spherical shape [$\pi(2\text{p-}0\text{h})$ states] the results become rather sensitive to even minor changes of the deformation parameters. For example, the single-particle structure changes from predominantly $p_{3/2}$ to $f_{5/2}$ when the deformation changes from $\beta_2=0.0$ to $\beta_2=0.1$. Another important point to be mentioned is that the negative parity states are governed by several subshells ($3p_{3/2}$,$2f_{5/2}$), and the results depend not only on the shape and/or mixing, but also on the accuracy of the position of the different spherical states involved. This is in contrast to the positive parity states where we deal with one shell only, the unique parity $i_{13/2}$.

According to PPR calculations for the oblate states of negative parity one expects $I=5/2^-$ as the lowest state in ^{191}Po. The $I=3/2^-$ state is calculated to be $\approx$50 keV higher in energy, both for neutron numbers 105 and 107. However, as mentioned above, one cannot unambiguously predict the sequence of the lowest-lying states in the case of negative parity states. Hence we used our new experimental data to get more insight into the possible configurations. In particular, assigning $3/2^-$ to ^{191}Po(l.s.) and to the 375 keV excited state in ^{187}Pb(l.s.) makes it possible to explain practically all experimental observations. First of all, in this case a strong $E0$ component in the 375 keV γ decay leads to $3/2^-$ spin and parity for the spherical ^{187}Pb(l.s.), in agreement with the low hindrance factor value for the corresponding α decay towards the daughter ^{183}Hg(l.s.); see the discussion in [16]. Furthermore, the α-decay pattern of the low-spin isomer in ^{191}Po can be understood by assuming mixing of the spherical $3p_{3/2}\otimes\pi(2\text{p-}0\text{h})$ with the deformed $3p_{3/2}\otimes\pi(4\text{p-}2\text{h})$ configurations in ^{191}Po(l.s.). As a result of this admixture, the feedings toward the spherical $3p_{3/2}\otimes\pi(0\text{p-}0\text{h})$ isomeric state and toward the oblate $3p_{3/2}\otimes\pi(2\text{p-}2\text{h})$ intruder state in the daughter ^{187}Pb have comparable strengths as seen from the hindrance factors of 2.9 and 1.6, respectively. The difference in the hindrance factor arises from the different overlap between the mixed $3/2^-$ state in ^{191}Po on the one hand and the spherical and oblate $3/2^-$ states in ^{187}Pb on the other.

In contrast, assuming $5/2^-$ as a spin and parity for ^{191}Po(l.s.) or for the 375 keV excited state in ^{187}Pb (or for both of them) leads to a number of contradictions with the experimental data (hindrance factor values, $E0$ multipolarity of the 375 keV decay) and therefore we rule out this possibility.

Finally, we would like to mention that recently two α-decaying isomeric states were distinguished for the first time in the lighter odd-mass nucleus ^{185}Pb [38]. By measuring the hyperfine splitting of the atomic levels, combined with the complementary α-decay data, the spin and parity of these isomeric states were experimentally deduced as $3/2^-$ and $13/2^+$. This confirms that the expected systematical occurrence of the $3/2^-$ and $13/2^+$ isomeric states in the odd-mass Pb nuclei still holds at least up to $N=103$.

3. Mixing in ^{191,193,195}Po and shape staggering in ^{191m,g}Po

A comment on the mixing of the different configurations in the even- and odd-mass polonium nuclei is appropriate here.

In the even-mass $^{190-198}$Po isotopes the reduced width of the α decay to the excited $0^+\,\pi(2p\text{-}2h)$ oblate intruder state relative to the decay to the $0^+\,\pi(0p\text{-}0h)$ spherical ground state in the daughter lead nuclei was found to evolve from 2.8 times slower in ^{198}Po to 2 times faster in ^{190}Po [11,39–42]. This is well understood from a theoretical point of view as a gradual transition from a nearly spherical $\pi(2p\text{-}0h)$ ground state in ^{198}Po and heavier polonium nuclei towards a

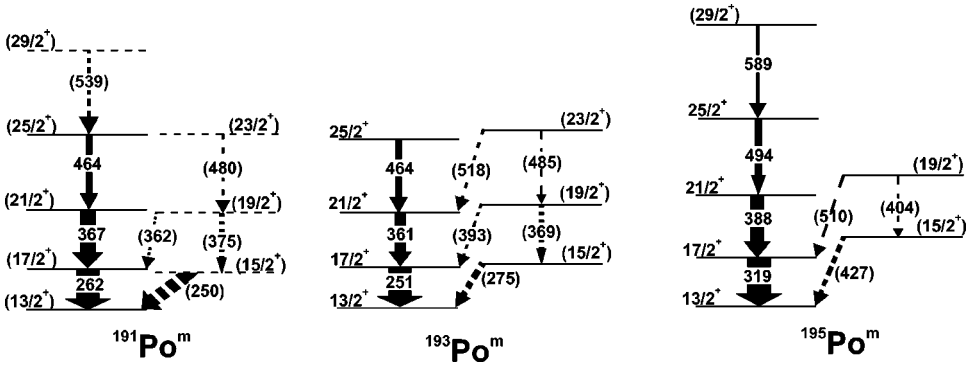

FIG. 8. Level schemes of ^{191m,193m,195m}Po; data for ^{193m,195m}Po are taken from [10].

mixed [spherical-oblate, $\pi(2p\text{-}0h)+\pi(4p\text{-}2h)$] ground state in the lighter ones with a dominant intruder $\pi(4p\text{-}2h)$ configuration in ^{190,192}Po [39,40,42].

One does not expect *a priori* that in the odd-mass Po $\rightarrow$Pb decay chain the odd neutron acts just as a spectator and that the α decay is simply a duplicate of the decay in the even-even neighbors. As known, for example, for the odd-mass Pt and Hg nuclei close to the midshell at $N=104$ [13,14], the coupling of different valence neutrons ($1i_{13/2}$ or $3p_{3/2}$) to the same even core produces different effects, in some cases driving the whole nucleus to deformation and/or leading to shape staggering between the corresponding configurations in the same nucleus.

Recently, fine-structure α decay to excited intruder configurations in the daughter lead nuclei has been observed both for the $3/2^-$ ground state and for the $13/2^+$ isomeric states of ^{193,195}Po. Preliminary data were presented in [43] and are discussed in detail in [44]. The decay patterns in all four cases (^{193m,g}Po and ^{195m,g}Po), along with those of $^{190-198}$Po, are similar to the case of ^{191g}Po: the decays to the excited intruder configuration have similar hindrance factor values (within a factor of 2–3), compared to the decays towards the corresponding ground states or isomeric states. Similar to the even-mass polonium nuclei, the decay pattern of the odd-mass isotopes ^{191g,193m,g,195m,g}Po is understood as a result of the mixing of the intruder and the normal configurations in the parent polonium nuclei [44].

In contrast, in ^{191m}Po a transition to a pure intruder π(4p-2h) configuration is clearly seen from the hindrance factors (see Sec. IV B 1) and half-life values of the α decay of ^{191m,g}Po. While the α-decay energies of the $3/2^-$ and $13/2^+$ states are different by $\approx$40 keV only, their half-life values differ by more than a factor of 4. As shown above (see also [16]), the large difference in half-life values is explained through the action of multiparticle multihole intruder orbitals, leading to a pronounced shape staggering between the $13/2^+$ and $3/2^-$ isomeric states in ^{191}Po. This inference is further confirmed by the γ-decay data discussed in the next section.

To our knowledge, this is the first case of shape staggering between the ground state and isomeric state in the same nucleus above the shell closure at $Z=82$. It is interesting that in this case the shape staggering has been observed between oblate and nearly spherical configurations, while below the $Z=82$ shell closure it is observed between oblate and prolate configurations (Pt, Hg nuclei) [13,14].

C. Transition towards the strong-coupling scheme in ^{191}Po(h.s.)

Figure 8 shows the known excited states, built on top of the assumed $13/2^+$ isomer in ^{191,193,195}Po. We remind that in all three cases the states within the unfavored band ($15/2^+$-$19/2^+$-$\cdots$) were placed on the basis of the energy sum and intensity relations only and therefore should be considered as tentative.

As discussed extensively in the literature the sequence of $13/2^+$-$17/2^+$-$21/2^+$-$\cdots$ states in the odd-mass Po nuclei can be described either by the weak coupling of the odd $i_{13/2}$ neutron to the neighboring nearly spherical even core (see, for example, [17] and references therein) or, within the rotational plus intruder framework [10], as a rotation alignment and decoupling of the $i_{13/2}$ neutron hole from the oblate core. The new data for favored and unfavored states in ^{191m}Po together with similar data on ^{193m,195m}Po [10] provide new insight into the structure of the odd-mass polonium nuclei close to the midshell at $N=104$. The observation of the favored and unfavored states and their behavior as a function of the mass number allows us to make a distinction between weak coupling and rotation aligned schemes. Indeed, although in both cases one expects to observe the favored $13/2^+$-$17/2^+$-$21/2^+$-$\cdots$ states with the core energy spacing, the behavior of the unfavored states will be different. The weak-coupling scheme is known to be valid for nearly spherical nuclei, and in addition to the favored $j,j+2,j+4,\ldots$ states one expects to see nearly degenerate multiplets of unfavored states with $|R-j|\leqslant I\leqslant|R+j|$ ($R=2,4,6,\ldots$ core rotational angular momentum), centered at the core energies (see [45,46] and references therein). Hence, in the weak-coupling scheme, there is no explicit dependence on the Fermi level, i.e., the Ω value of the odd particle. On the other hand, in the rotationally aligned scheme the position of the unfavored states relative to the favored ones changes depending on the position of the Fermi surface and therefore on the magnitude of the Coriolis interaction. For a particle having angular momentum j, in a nucleus with spin I and moment of inertia $\mathfrak{I}$ the Coriolis force is $V_{Cor}\approx-2(\hbar^2/2\mathfrak{I})Ij$ [45] and the strongest Coriolis effects arise for the high-j, low-Ω orbitals. Therefore in the case of the odd-mass polonium nuclei with $A\leqslant197$ (opening of the $i_{13/2}$

orbital) the coupling of the $1i_{13/2}$ hole state (small Ω value) should result in a decoupled band of the $13/2^+$-$17/2^+$-$21/2^+$-$\cdots$ favored states, while the unfavored states ($15/2^+$-$19/2^+$-$23/2^+$-$\cdots$) should lie higher in energy [45,47]. By depleting the $i_{13/2}$ orbital (increasing the Ω value) the Coriolis interaction will decrease and hence the unfavored states come down in energy until they are equally spaced between the favored states. Such a band is considered as the manifestation of the so-called strong-coupling scheme, which is valid at somewhat larger deformations [45].

This is exactly what one observes experimentally: for $A(Po) \geqslant 198$ the pattern of the excited states in the near-spherical even- and odd-mass nuclei can be well described by the weak-coupling scheme [10,17]. Then, around $A = 198$ (opening of the $i_{13/2}$ orbital) the downward behavior of the excited states indicates a transition to more deformed configurations corresponding to the rotationally aligned scheme. Finally, in ^{191m,193m,195m}Po the unfavored states are tentatively observed, their excitation energy lowers with decreasing mass number, and in ^{191m}Po for the first time they are found below the states of the favored band.

Therefore, we conclude that the pattern, shown in Fig. 8, provides tentative evidence for a change towards the strong-coupling scheme in the odd-mass Po nuclei by approaching the neutron midshell at $N = 104$. It also supports the onset of oblate deformation in ^{191m}Po, in agreement with the results of complementary α-decay studies and the results of PES and PPR calculations.

D. Excited states and shape coexistence in ^{187}Pb

We remind the reader that in the neighboring even-mass ^{186,188}Pb nuclei coexisting oblate $\pi(2\text{p-}2\text{h})$ and prolate $\pi(4\text{p-}4\text{h})$ configurations have been predicted by PES calculations at about 1 MeV above the spherical ground state with a rather small energy separation between the deformed 0^+ bandheads (see, for example, [42] and references therein). As an example, in a recent α-decay study of ^{190}Po these bandheads have been observed in the daughter ^{186}Pb isotope at an excitation energy of about 600 keV with an energy separation of about 120 keV only [42]. Although the predicted excitation energies are higher than the experimental ones, the prediction that the oblate bandhead is lowest in energy is confirmed by the experiment. As discussed in Sec. IV A, the difference in correlation energy could be responsible for the quantitative discrepancies.

In the odd-mass lead nuclei, the coupling of the odd neutron to the states in the spherical, oblate, and prolate minima of the neighboring even core should also result in coexisting states belonging to different minima. However, a dramatic change of the relative positions of different configurations can arise as known in the case of the odd-mass Pt and Hg nuclei by approaching the midshell at $N = 104$ (see discussion and references in Sec. IV B).

1. Negative parity states

The potential-energy surface for the negative parity states in ^{187}Pb is given in Fig. 7(f). The coupling of the negative parity neutron to the even-even Pb core leads to coexistence of three different shapes with the nearly spherical one lowest in energy. The prolate and oblate bandhead states are predicted at the excitation energies of 370 keV and 540 keV, respectively, thus by about 600 keV lower than the corresponding calculated minima in the even-even case. In Sec. IV B 2, based on the hindrance factor values, we interpreted the observed excited state at 375 keV as a $3/2^-$ bandhead of the oblate configuration. We could not identify the predicted prolate bandhead state, presumably due to the fact that α decay from nearly spherical ^{191}Po(l.s.) to this state would be more strongly hindered, as it would involve a two-step process. For the negative parity states one can conclude that both theoretically and experimentally one observes a strong lowering of the deformed minima in the low-spin isomer in ^{187}Pb relative to the even-mass neighbors.

2. Positive parity states

The results of the PES calculations for the positive parity states in ^{187}Pb are given in Fig. 7(e). Both deformed bandhead states are expected at about 800 keV above the spherical minimum. Similarly to the negative parity states, the coupling of the odd neutron ($1i_{13/2}$) to the even-even core leads to the lowering of the deformed minima in comparison with the even-even case. Also experimentally the excited states, identified in this work in the high-spin isomer in ^{187}Pb, lie around 500 keV, thus lower than the 0^+ bandhead states in the even-even nuclei. The quantitative agreement with the PES calculations is reasonable and may reflect the difference in correlation energy.

The identification of the state at 494 keV (presumably, $13/2^+$) in ^{187}Pb(h.s.) as a band head in the oblate minimum was already discussed in Sec. IV B.

It is well known that the α decays feeding to the low-lying members with $\Delta L \leqslant 2$ of the same rotational band have quite similar hindrance factor values, relative to the decay to the bandhead [4]. Furthermore, quite often in the absence of (or with weak) mixing with possible coexisting configurations, the states of the band are predominantly connected by the prompt intraband decays, rather than by the possible interband decays to coexisting structures. For example, in ^{192,194,196}Pb, the $B(E2{:}2^+_{2,obl}\text{-}0^+_{2,obl})/B(E2{:}2^+_{2,obl}\text{-}0^+_{1,sph})$ ratios between the intraband and interband decays, respectively, were found to be 358 in ^{196}Pb, 30 in ^{194}Pb and 5 in ^{192}Pb (see details in [48]). There is practically no mixing between the coexisting oblate and spherical configurations in ^{196}Pb, which results in the rather high value of this ratio. The smaller ratios in the lighter isotopes were explained by the increased mixing between the closely lying oblate and spherical 2^+ states [48] . Similar arguments are expected to be valid in the odd-mass Pb nuclei and were used in our study to search for the states, belonging to the oblate band, built on top of the $13/2^+$ state.

As was shown in Sec. IV B 1, based on the PPR calculations, we expect the $11/2^+$, $9/2^+$, and $15/2^+$ states of the oblate band to lie above the $13/2^+$ bandhead by about 10 keV, 50 keV, and 170 keV, respectively. The excitation energy of the state at 573(15) keV relative to the $13/2^+_2$ state at 494 keV is 80(15) keV, which is quite close to the calculated

value of 50 keV for the expected $9/2^+$ state. The deduced $E2$ multipolarity for the (unobserved, presumably strongly converted) 80(15) keV transition also suggests a spin and parity assignment of $I^\pi = 9/2^+$ for this state. Furthermore, a rather low hindrance factor of 2.1(5) for the feeding 6815(15) keV decay *relative* to the 6888 keV transition, feeding the state at 494 keV, also points that these states belong to the same band. Finally, assuming an upper limit of $\leqslant 1$ counts for the number of unobserved 6815-573 keV coincident pairs and pure $E2$ multipolarity for the 80 keV and 573 keV transitions, an upper limit of $B(E2{:}9/2^+ \rightarrow 13/2^+_{2,obl})/B(E2{:}9/2^+ \rightarrow 13/2^+_{1,sph}) \geqslant 450$ can be given for the ratio between the decay strengths for the 80 keV and 573 keV decays. As above, the number of the 6815-80 keV decays was estimated from the number of 6815-494 keV decays, as the 80 keV and 494 keV transitions are in a prompt cascade. The rather high value of this ratio suggests that the state at 573 keV has a rather pure configuration, which is similar to the one of the oblate $13/2^+_2$ state at 494 keV, but different from the spherical $13/2^+_1$ state in ^{187}Pb.

On these grounds we interpret the excited state at 573 keV in ^{187}Pb(h.s.) as a $9/2^+$ member of the oblate band, built on the $13/2^+$ bandhead at 494 keV. We do not observe an expected $11/2^+$ oblate state, which is predicted at about 10 keV only above the oblate bandhead. As a result of uncertainty in the calculations, the actual excitation energy may be a bit different, but it should lie below the assumed $9/2^+$ state. Therefore, the following arguments should be still valid practically irrespectively of the actual position of the $11/2^+$ state. First of all, like the $13/2^+ \rightarrow 9/2^+$ decay at 6815 keV, the expected $13/2^+ \rightarrow 11/2^+ \alpha$ decay ($\approx$6878 keV) to the $11/2^+$ state would involve an angular momentum change of $\Delta L = 2$ and therefore should be hindered quite similarly to the former one. Furthermore, the coincident intraband prompt low-energy $11/2^+ \rightarrow 13/2^+$ pure $M1$ or mixed $M1/E2$ transition should be strongly converted [$\alpha(\text{tot,theor.},M1) = 293$, $\alpha(\text{tot,theor.},E2) = 9 \times 10^4$ [26]], resulting in the full α-e^- summing in the Si detector. As a result of all this, it is impossible to separate the $\approx$6878 keV and the 6888 keV decays in the singles α spectrum of Fig. 1. Also, in the two-dimensional α-γ plot (Fig. 2) the former decays will only add to the 6888-494 keV decays, similar to the case of 6815-494 keV decays.

The nonobservation of the 6815(15)-472 keV coincident pairs rules out that there is a prompt direct or cascade (via the state at 494 keV) decay from the state at 573 keV to the state at 472 keV. This fact strongly suggests that the latter state is not a member of the oblate band to which the 494 keV and 573 keV states have been attributed. This is further supported by a relatively large difference of 12(4) between the hindrance factor values for the 6888 keV and 6909 keV α decays, feeding the 494 keV and 472 keV excited states, respectively. Therefore, the latter state could be tentatively interpreted as a state in the prolate minimum. Such an interpretation would be in agreement with the results of the PES calculations, which suggest that the prolate- and oblate-deformed minima should have quite similar excitation energies for the positive parity states in ^{187}Pb; see Fig. 7(e). In the *prolate* minimum PPR calculations predict the $9/2^+[624]$ Nilsson state to be lowest in energy with a rotational band built on top of it. We note that the prolate $9/2^+[624]$ bandhead is well established in the lighter isotones [4]. Therefore, one could tentatively assign the state at 472 keV as the $9/2^+$ bandhead of the prolate band. However, as a result of a lack of definitive proof and relatively low statistics, no solid conclusions can be drawn here.

As a result of low statistics and a large uncertainty of the hindrance factor value for the 6790 keV α decay, we prefer not to make any conclusions on the nature of the 594 keV state.

We also point out the nonobservation in [49,50] of the decays from the presumably spherical $17/2^+$ state at 831 keV, observed in an in-beam study of ^{187}Pb, to any of the states, observed in this work. Clearly, the direct decays to the suggested $9/2^+$ and (unobserved) $11/2^+$ states of the oblate band would be strongly retarded simply due to high multipolarity for the corresponding γ transitions. In contrast to this, the $17/2^+ \rightarrow 13/2^+_2$ $E2$ decay to the state at 494 keV should be expected if the 831 keV and 494 keV states belonged to the same band. Therefore, the nonobservation of this transition suggests that the $17/2^+$ and $13/2^+_2$ states belong to different configurations, in agreement with the spherical and oblate interpretation for these two states, suggested in [49] and in this work, respectively. We note that according to PPR calculations, an oblate $17/2^+$ state is expected at about 260 keV above the bandhead, thus at the excitation energy of 754 keV in ^{187}Pb (h.s.).

The same arguments can be applied to the decay from the 831 keV state to the state at 472 keV, tentatively assigned in this work as the $9/2^+$ prolate bandhead. Although a direct decay to this state is prohibited, feeding through the higher-lying states of the band, which are predicted at about 572 keV ($13/2^+$), 680 keV ($15/2^+$), and 802 keV ($17/2^+$), could be possible. The nonobservation of such decays in [49,50] suggests that the states at 831 keV and 472 keV have different configurations, which indirectly confirms the prolate assignment of the latter state.

Therefore, the observation in ^{187}Pb of the oblate bandhead at 494 keV and, tentatively, of the prolate bandhead at 472 keV, along with the observation of the spherical ground state, provides first, although, tentative, evidence for triple spherical-oblate-prolate shape coexistence at low energy in the odd-mass lead nuclei.

It is interesting to note that in case the state at 472 keV is indeed a bandhead of the prolate configuration, three coexisting $17/2^+$ states should be expected at nearly the same excitation energy: the observed (presumably) spherical state at 831 keV and (unobserved) oblate and prolate states at 754 keV and 802 keV, respectively.

V. SUMMARY

Complementary α- and γ-decay studies of the neutron-deficient nucleus ^{191}Po have been performed at the RITU gas-filled separator. Improved α-decay data confirm the ob-

servation of shape staggering between two isomeric states in ^{191}Po (presumably $13/2^+$ and $3/2^-$) and provide evidence for oblate deformation of the $13/2^+$ isomeric state. This conclusion is supported by the results of the prompt in-beam study of the $13/2^+$ isomeric state, on top of which, as in the cases of ^{193m,195m}Po, favored and (tentatively) unfavored excited states have been observed. For the first time in the odd-mass polonium nuclei the states of the unfavored band, based on the $1i_{13/2}$ neutron, come down in energy below the states of the favored band, built on the same neutron. This tentatively indicates an evolution towards a strong-coupling scheme and a rotational-like band for ^{191m}Po. These conclusions are consistent with the predictions of potential-energy surface and particle-plus-rotor calculations, which provide a good description of the observed data.

Recently a flattening of the energy systematics of the excited states in the even-mass polonium nuclei around $N=108$ has been observed [8–10]. This confirms the conclusion, drawn from the fine-structure α-decay studies [39–42], that the intruder $\pi(4p\text{-}2h)$ configuration becomes the dominant configuration in the ground state of the even polonium nuclei close to $N=108$. From our data on the odd-mass Po isotopes a similar flattening of the systematics of the excited states built on top of the $13/2^+$ isomer has been deduced. Therefore, the importance of the $\pi(np\text{-}mh)$ intruder configurations in the low-energy states of the odd-mass polonium nuclei around $N=108$ can be confirmed.

Within the experimental accuracy the $13/2^+$ and $3/2^-$ isomeric states become degenerate in ^{187}Pb. This is what one expects from the systematics of the Pb isotopes, since one is moving more deeply into the spherical $i_{13/2}$ shell.

The observation of the low-lying oblate excited states at 494 keV and 573 keV and, presumably, prolate excited state at 472 keV, along with the spherical ground configuration in the high-spin isomer of ^{187}Pb, can be tentatively interpreted as evidence for the triple spherical-oblate-prolate coexistence at low energy in this nucleus. A possible near degeneracy of the three coexisting $17/2^+$ states in ^{187}Pb (h.s.) has also been pointed out.

ACKNOWLEDGMENTS

This work was supported by the Academy of Finland under Finnish Center of Excellence Program 2000-2005 (Project No. 44875, Nuclear and Condensed Matter Physics Program at JYFL), the Access to Large Scale Facility program under the Training and Mobility of Researchers program of the European Union, by the FWO-Vlaanderen, and by the GOA (Onderzoeksprogramma K.U.Leuven) and IUAP program (Belgium) and the Swedish Natural Research Foundation (NFR). A.N.A. was partially supported by the EXOTAG project, HPRI-1999-CT-50017. K.V.d.V. is Research Assistant of the FWO-Vlaanderen.

[1] A. Oros *et al.*, Nucl. Phys. **A645**, 107 (1999).
[2] R. Julin, K. Helariutta, and M. Muikku, J. Phys. G **27**, R109 (2001).
[3] A. N. Andreyev *et al.*, *Proceedings of the International Symposium on Nuclear Physics*, Gottingen, Germany, 2001 (World Scientific, Singapore, 2001), p. 231.
[4] R. B. Firestone *et al.*, *Table of Isotopes*, 8th ed. (Wiley, New York, 1996).
[5] A. Maj *et al.*, Z. Phys. A **324**, 123 (1986).
[6] D. Alber *et al.*, Z. Phys. A **339**, 225 (1991).
[7] G.D. Dracoulis *et al.*, Phys. Rev. C **63**, 061302(R) (2001).
[8] K. Helariutta *et al.*, Phys. Rev. C **54**, R2799 (1996).
[9] N. Fotiades *et al.* Phys. Rev. C **55**, 1724 (1997).
[10] K. Helariutta *et al.*, Eur. Phys. J. A **6**, 289 (1999).
[11] N. Bijnens *et al.*, Phys. Rev. Lett. **75**, 4571 (1995).
[12] N. Bijnens *et al.*, Phys. Rev. C **58**, 754 (1998).
[13] F. Le Blanc *et al.*, Phys. Rev. C **60**, 054310 (1999).
[14] G. Ulm *et al.*, Z. Phys. A **325**, 247 (1986).
[15] J. Wauters *et al.*, Phys. Rev. C **47**, 1447 (1993).
[16] A.N. Andreyev *et al.*, Phys. Rev. Lett. **82**, 1819 (1999).
[17] N. Fotiades *et al.*, Phys. Rev. C **56**, 723 (1997).
[18] M. Leino *et al.*, Nucl. Instrum. Methods Phys. Res. B **99**, 653 (1995).
[19] A.N. Andreyev *et al.*, Eur. Phys. J. A **6**, 381 (1999).
[20] H. Kettunen *et al.*, Acta Phys. Pol. B **32**, 989 (2001).
[21] R.S. Simon *et al.*, Z. Phys. A **325**, 197 (1986).
[22] E.S. Paul *et al.*, Phys. Rev. C **51**, 78 (1995).
[23] J.O. Rasmussen, Phys. Rev. **113**, 1593 (1959).
[24] Nuclear Data Sheets **15**(2), VI (1975).
[25] GEANT detector simulation tool, http://wwwinfo.cern.ch/asd/geant, CERN, Geneva, 1993.
[26] Program to calculate conversion coefficients, National Nuclear Data Center (NNDC), http://www.nndc.bnl.gov/nndc/physco
[27] P. Misaelidis *et al.*, Z. Phys. A **301**, 199 (1981).
[28] V.M. Strutinsky, Yad. Fiz. **3**, 614 (1966).
[29] S. Cwiok *et al.*, Comput. Phys. Commun. **46**, 379 (1987).
[30] H.C. Pradhan, Y. Nogam, and J. Law, Nucl. Phys. **A201**, 357 (1973); W. Satula, R. Wyss, and P. Magierski, *ibid.* **A578**, 45 (1994).
[31] W. Satula and R. Wyss, Phys. Scr. **56**, 159 (1995).
[32] A.M. Baxter *et al.*, Phys. Rev. C **48**, 2140 (1993).
[33] J. Heese *et al.*, Phys. Lett. B **302**, 390 (1993).
[34] J.F.C. Cocks *et al.*, Eur. Phys. J. A **3**, 17 (1998).
[35] Th. Hilberath *et al.*, Z. Phys. A **342**, 1 (1992).
[36] J. Rikovska, R. Wyss, and P. Semmes, Hyperfine Interact. **75**, 59 (1992).
[37] P. Ring and P. Schuck, *The Nuclear Many-Body Problem* (Springer-Verlag, New York, 1980).
[38] A. N. Andreyev, Eur. Phys. J. A **14**, 63 (2002).
[39] N. Bijnens *et al.*, Z. Phys. A **356**, 3 (1996).
[40] R.G. Allatt *et al.*, Phys. Lett. B **437**, 29 (1998).
[41] A.N. Andreyev *et al.*, J. Phys. G **25**, 835 (1999).
[42] A.N. Andreyev *et al.*, Nature (London) **405**, 430 (2000).
[43] A.N. Andreyev *et al.*, in *Experimental Nuclear Physics in Europe*, edited by Berta Rubio *et al.*, AIP Conf. Proc. No. 495 (AIP, Melville, NY, 1999), p. 121.

[44] K. Van de Vel, Phys. Rev. C **65**, 064301 (2002).
[45] F.S. Stephens, Rev. Mod. Phys. **47**, 43 (1975).
[46] K. Heyde *et al.*, Phys. Rep. **102**, 291 (1983).
[47] R. F. Casten, *Nuclear Structure from a Simple Perspective* (Oxford University Press, New York, 1990), pp. 300–312.
[48] P. Van Duppen *et al.*, Phys. Rev. C **35**, 1861 (1987).
[49] A.M. Baxter *et al.*, Phys. Rev. C **58**, 2671 (1998).
[50] G. D. Dracoulis (private communication).